Available online at www.sciencedirect.com

SciVerse ScienceDirect

Scripta Materialia 65 (2011) 1002–1005

Scripta MATERIALIA

www.elsevier.com/locate/scriptamat

Flat to slant ductile fracture transition: Tomography examination and simulations using shear-controlled void nucleation

T.F. Morgeneyer* and J. Besson

Mines ParisTech, Centre des Matériaux, UMR CNRS 7633, BP87, 91003 Evry cedex, France

Received 17 July 2011; revised 11 August 2011; accepted 1 September 2011
Available online 8 September 2011

Tomography examination of arrested cracks at crack initiation, flat to slant transition and slant propagation indicates a clear change in micromechanisms from high-stress triaxiality void growth to shear-dominated coalescence in the slant regime. A Gurson-type model is used and a shear void nucleation term based on the Lode parameter for strain rate is suggested for simulation of a fully meshed sample, which achieves flat to slant crack transition at loads close to experimental results for aluminium.

Keywords: Flat fracture; Slant fracture; Lode parameter; Shear; X-ray tomography

In the ductile fracture of sheet material, fracture initiation at the notch or precrack root typically commences with the formation of a flat triangular region (i.e. the normal to the crack corresponds to the loading direction) [1]. In this area, large primary dimples are observed on the fracture surfaces. Once the initial triangle is formed, the crack tilts and becomes slanted, forming an angle of approximately 45° with the loading direction. Here, the primary dimples are observed, together with secondary dimples. Near the notch root of severely notched samples, the mean stress is higher, and this promotes void growth [2]. Experimental results indicate that, in the slant fracture region, fracture is dominated not by growth of primary voids nucleated on large constituent particles, but by shear void sheeting mechanisms involving the growth and coalescence of voids nucleated at dispersoids (submicron-sized particles introduced in the alloy to control grain growth [3,4]) or by fracture on grain boundaries [5]. In recent studies, the behaviour of voids has been studied numerically under shear loading, showing weak volume change and strong shape change [6].

In a finite element study [7], the crack propagation of both a meshed flat and a slant crack was investigated. The stress fields ahead of the respective cracks during crack propagation under remote mode I loading were compared and it was identified that for a slant crack the constraint and the mean stress ahead of the crack are reduced whilst the effective stress is augmented compared to a flat crack. This promotes a shearing type of fracture.

Modelling of the flat to slant fracture transition is hard to perform and the fracture path is often only reproduced as flat fracture [2,8]. Attempts have been made to reproduce the flat to slant fracture transition [10–12], but the fracture path and the macroscopic load could not be reproduced simultaneously. Often a comparison with experimental results is missing in the literature. Recent models try to extend the Gurson model, which correctly describes void growth at high levels of stress triaxiality, to cases of fracture at low levels of stress triaxiality [13]. The Lode parameter is often used to identify the occurrence of shear [12,14] and will also be used in the present study.

Here, new insight into flat to slant fracture transition are gained via tomography observation of arrested cracks. A Gurson model extension using a shear nucleation term via using the strain rate tensor Lode parameter is presented and simulations are shown.

Aluminium AA2139 sheets were supplied by Alcan CRV with a thickness of 3.2 mm in a commercial T351 condition, i.e. solution treated, stretched and naturally aged. Testing was performed in L (rolling direction)–T (long transverse) configuration. For further details on materials microstructure and mechanical properties the reader is referred to Refs. [8,9].

For synchrotron radiation-computed tomography (SRCT) observations, three different L–T Kahn tear tests

* Corresponding author. Tel.: +33 160763061; fax: +33 160763150; e-mail: thilo.morgeneyer@mines-paristech.fr

1359-6462/$ - see front matter © 2011 Acta Materialia Inc. Published by Elsevier Ltd. All rights reserved.
doi:10.1016/j.scriptamat.2011.09.004

[15] were arrested at different loads: before final failure of the coupon at peak load (1), at the flat to slat crack transition (2) and at the slant fracture (3) (see Fig. 1). SRCT was performed at beamline ID 19 of the European Synchrotron Radiation Facility (ESRF), Grenoble, France, at 20.5 keV. An isotropic voxel size of 0.7 μm was obtained in the reconstructed slices. Sample cutting around the mid-thickness is described in Ref. [9].

Figure 2 shows two-dimensional (2-D) sections of SRCT data with the crack propagation direction normal to the image plane. It can be clearly seen that for crack interruption at peak load (arrow 1 in Fig. 1) no macroscopic crack has formed but substantial void growth has taken place ahead of the machined notch (see Fig. 2(a)) in a band normal to the loading direction. For crack interruption in the flat to slant crack transition regime (arrow 2 in Fig. 1, Fig. 2(b)), the flat crack, oriented normal to the former loading direction, is wide open and substantial void growth has taken place. However, in the slanted area of the crack only very limited void growth can be seen. The limited void growth and narrow crack opening are also seen for the arrested crack in the propagation region (Fig. 2c). The observations of decreasing void growth are consistent with the decrease in stress triaxiality that takes place after crack initiation [2] and clearly indicates a change in fracture mechanisms between flat and slant fracture from high stress triaxiality void growth to lower stress triaxiality shear mechanisms.

In general terms, shear is thought to play a major role for the flat to slant transition and for ductile fracture. Thus, a way to incorporate shear fracture in the Gurson model framework is developed here. The aim is to add the nucleation of a second population of small voids as a function of the encountered stress state and, in particular, shear. As shown in recent models [12,14], the Lode parameter may be an adequate indicator for shear. Here, the Lode parameter for strain rates, $\mu_{\dot{p}}$, is used based on the idea that it is the deformation rate in a shear configuration that may cause shear and slant fracture. A similar idea has been suggested in Ref. [14], where coalescence is suggested to occur at shear fracture. However, this model has not been applied to structures.

The shear-controlled void nucleation rate depends on the Lode parameter of the plastic strain rate tensor, $\mu_{\dot{p}}$, which is computed as:

$$\mu_{\dot{p}} = \frac{\dot{p}_2}{\dot{p}_1 - \dot{p}_3} \quad \text{with } \dot{p}_1 \geqslant \dot{p}_2 \geqslant \dot{p}_3 \tag{1}$$

where $\dot{p}_1 \geqslant \dot{p}_2 \geqslant \dot{p}_3$ are the principal values of the plastic strain rate tensor.

The shear-controlled nucleation rate is then expressed as:

$$A_{n_2} = \begin{cases} A_{0_2} \cdot \exp\left(-\left(\frac{\mu_{\dot{p}}}{\mu_{\dot{p}0}}\right)^2\right) & \text{if} \quad p > p_{c_2} \\ 0 & \text{otherwise} \end{cases} \tag{2}$$

where A_{0_2}, p_{c_2} and $\mu_{\dot{p}_0}$ are parameters that need to be adjusted. The chosen function is such that secondary nucleation is maximum when $\mu_{\dot{p}}$ is close to 0, which corresponds to one direction being under plane strain ($\dot{p}_2 \simeq 0$). Under this state, band location is easier than under quasi-axisymmetric deformation (i.e. $\dot{p}_2 \simeq \dot{p}_3 \simeq -\frac{1}{2}\dot{p}_1$ and $\mu_{\dot{p}} = \pm\frac{3}{2}$), as shown in Ref. [16]. It is therefore assumed that easier localization under plane strain will lead to nucleation in a population of small secondary inclusions (such as dispersoids) and failure by void sheeting [3]. This mechanism leads to a very small actual void volume fraction but to highly detrimental damage. This is described by a large value of parameter A_{0_2}. Note that, in the case of an isotropic von Mises incompressible material, $\mu_{\dot{p}}$ corresponds to the Lode factor computed using the stress deviator as it is co-linear with the plastic strain rate tensor. This then corresponds to the Lode parameter dependence proposed in Refs. [14,17]. It is believed that the use of the Lode parameter of the plastic strain rate tensor is more appropriate in the case of anisotropic materials [8].

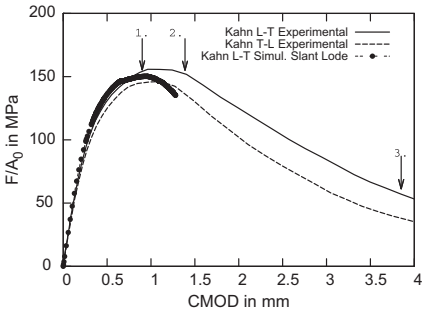

Figure 1. Kahn tear test results for L–T and T–L testing orientations [8]. Arrows indicate the three different points where tests have been arrested for tomography observation; simulation results for flat to slant fracture using shear nucleation controlled by the Lode parameter for the strain rate.

In the framework of the Gurson model, the following equation for nucleation of voids on secondary phases is often used:

$$\dot{f}_{n_i} = A_{n_i}\dot{p} \tag{3}$$

where $\dot{f}_{n_i}$ is the void nucleation rate, $\dot{p}$ is the strain rate and A_{n_i} may be any positive function of the state variables. Primary void nucleation corresponding to nucleation of the void around coarse intermetallic particles ($\dot{f}_{n_1}$) is calculated as in Ref. [8], supposing nucleation of voids around these particles up to 10% strain.

The classic Gurson potential is used:

$$\Phi = \frac{\sigma_{eq}^2}{\sigma_f^2} + 2q_1 f_* \cosh\left(\frac{q_2}{2}\frac{\sigma_{kk}}{\sigma_f}\right) - 1 - q_1^2 f_*^2 = 0 \tag{4}$$

where σ_f is the flow stress of the matrix, σ_{eq} is the von Mises stress, σ_{kk} is the trace of the stress tensor and f_* is the void volume fraction, which represents the increased damaging effect of voids during coalescence [18]. f_* is calculated here as in Ref. [8]. In order to enhance the Gurson model, two fitting parameters (q_1,q_2) [19] that influence the void growth were introduced by Tvergaard [18]. q_1 and q_2 were identified here via 2-D anisotropic void shape cell calculations using a elasto-plastic material law identified on an L direction tensile test (see also Ref. [8]).

The following equation is used for isotropic hardening, with a yielding criterion close to the Tresca criterion [8]:

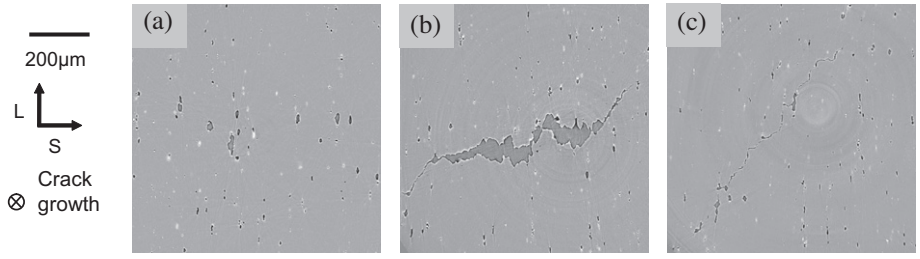

Figure 2. 2-D SRCT section (normal to crack propagation direction) of arrested L–T Kahn tear tests: (a) at peak load, no crack has been formed yet (arrow 1 in Fig. 1); (b) in the flat to slant transition regime (arrow 2 in Fig. 1); and (c) in the slanted crack propagation (arrow 3 in Fig. 1).

Table 1. Parameters for simulation of flat to slant fracture.

Nucleation for shear				
A_{0_2}	$\mu_{\dot{p}_0}$	p_{c_2}		
2.0	0.011	0.1		
Void growth		*Damage*		
q_1	q_2	f_0	A_{n_1}	p_{c_1}
1.97	0.91	0.33%	0.045	0.1
Elastic–plastic behaviour				
E (GPa)	ν	R_0 (MPa)	K_0	
70	0.3	330	0.1018	
K_1	k_1	K_2	k_2	
0.7618	8.25	0.01109	11.8	

$$\sigma_f = R_0[1 + K_0 p + K_1(1 - e^{-k_1 p}) + K_2(1 - e^{-k_2 p})] \quad (5)$$

The shear nucleation parameters were found via trial-and-error calculations using a quarter sample with a coarser mesh than shown here.

The simulations have been carried out with the parameters given in Table 1 and using a fully meshed (3-D) sample, with a slightly tilted mesh to introduce an asymmetry. The modified Gurson–Tvergaard–Needleman (GTN) model was implemented using the finite element (FE) software Zebulon, developed at Mines ParisTech [20]. The element sizes in the finely meshed region were 50 μm in the T, 100 μm in the S and 53 μm in the element height (L) direction.

The 3-D FE mesh of the Kahn tear test sample is shown in Figure 3a, with a magnified image of a finely meshed crack initiation zone that has been slightly tilted to make the mesh asymmetric and favour slant fracture in one plane. Figure 3b shows the result with respect to the crack path of the simulation using the shear-controlled void nucleation term: the broken elements are made transparent and the flat to slant crack transition that reproduces the experimentally found crack path can be clearly seen. The crack front is shown in Figure 3c, with a view in the loading direction of the broken elements. It can be seen that the crack front has straightened at the slant fracture, consistent with experimental findings [1,9]. Figure 3c shows the results of the simulation only using the Gurson model results. The crack path remains flat throughout the entire crack propagation in this case, and substantial tunnelling takes place (Fig. 3d and e) that is only found experimentally at crack initiation [8] and is linked to the higher levels of stress triaxiality found at the sample centre that favours

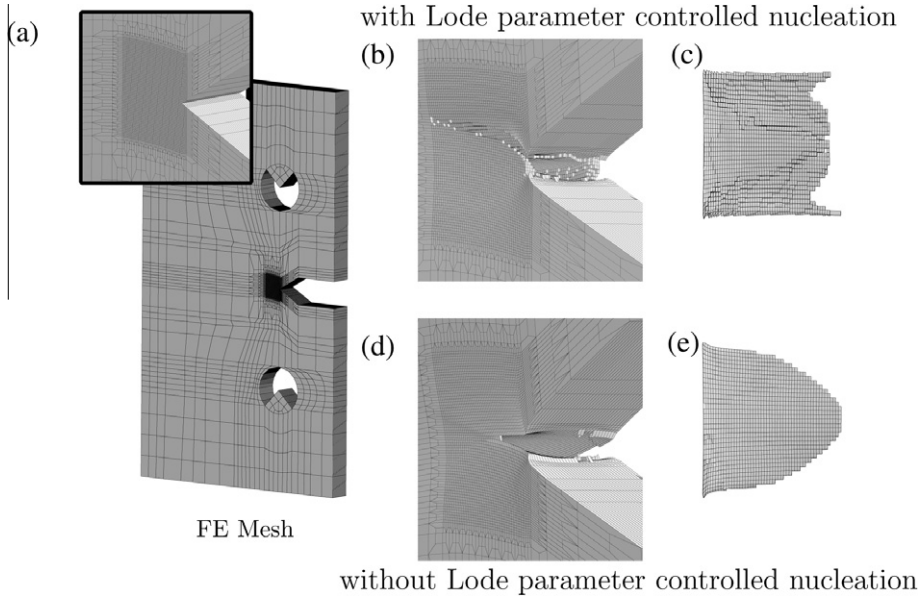

Figure 3. (a) 3-D tilted mesh of the Kahn tear test sample; (b) flat to slant fracture path for shear-controlled nucleation; (c) crack front for shear-controlled nucleation (viewed in the loading direction); (d) flat crack path for GTN only simulation; and (e) crack front for GTN only simulation (viewed in the loading direction).

void growth. However, this does not seem to be the prevalent fracture mechanism during slant fracture.

Figure 1 shows the structural response for L–T configuration simulation. The loads are predicted correctly up to the maximum. However, the load decrease in the flat to slant fracture simulation using the Lode strain rate parameter starts at a lower crack mouth opening displacement than in the experiment, so the simulation results for the L–T configuration are close to the experimental results for T–L loading. This also means that simulated loads are in the range of the experimental results, which represents an advantage compared to other attempts made to model slant fracture (e.g. [10,12]) that did not fit experimental results or that were not compared to them.

These results show that accounting for shear fracture processes may lead to a better comprehension and prediction of slant fracture, the flat to slant transition and low stress triaxiality ductile fracture in general. The strong points of the model modification presented here are that predicted loads are in a reasonable range compared to simulations. The modification can easily be implemented in a Gurson model. However, three new parameters, $\mu_{\dot{p}_0}$, A_{0_2} and p_{c_2}, need to be fitted, which may be time consuming as computation times are long. A fine mesh needs to be used to approximate the slanted fracture path. With progress in simulation techniques, such as parallel computing, remeshing and non-local modelling, these limitations may be overcome and the presented model may be used more easily for further valuable shear fracture comprehension.

The authors acknowledge Alcan CRV for material supply. Ian Sinclair, Marco Starink, Frederic Bron and Bernard Bes are thanked for technical discussion. The authors also thank Elodie Boller at ESRF ID19 for support with the microcomputed tomography.

[1] U. Zerbst, M. Heinimann, C. Dalle Donne, D. Steglich, Eng. Fract. Mech. 76 (2009) 5–43.
[2] F. Bron, J. Besson, Eng. Fract. Mech. 73 (2006) 1531–1552.
[3] W.M. Garrison, N.R. Moody, J. Phys. Chem. Solids 48 (1987) 1035–1074.
[4] F. Bron, J. Besson, A. Pineau, Mater. Sci. Eng. A. 380 (2004) 356–364.
[5] T.F. Morgeneyer, M.J. Starink, S.C. Wang, I. Sinclair, Acta Mater. 56 (2008) 2872–2884.
[6] V. Tvergaard, K.L. Nielsen, J. Mech. Phys. Sol. 58 (2010) 1243–1252.
[7] E. Mahgoub, X. Deng, M.A. Sutton, Eng. Fract. Mech. 70 (2003) 2527–2542.
[8] T.F. Morgeneyer, J. Besson, H. Proudhon, M.J. Starink, I. Sinclair, Acta Mater. 57 (2009) 3902–3915.
[9] T.F. Morgeneyer, M.J. Starink, I. Sinclair, Acta Mater. 56 (2008) 1671–1679.
[10] J. Besson, D. Steglich, W.B. Brocks, Int. J. Solids Struct. 38 (2001) 8259–8284.
[11] L. Xue, J. Int. J. Solids Struct. 44 (2007) 5163–5181.
[12] L. Xue, T. Wierzbicki, Eng. Fract. Mech. 75 (2008) 3276–3293.
[13] T. Pardoen, Comp. Struct. 84 (2006) 1641–1650.
[14] K. Nahshon, J.W. Hutchinson, Eur. J. Mech. 27A (2008) 1–17.
[15] ASTM-international, Standard B 871-01 (2001).
[16] A. Needleman, J. Rice, in: D.P. Koistinen (Ed.), Mechanics of Sheet Metal Forming, Plenum Publishing Corporation, New York, 1978, pp. 237–267.
[17] Y. Bai, T. Wierzbicki, Int. J. Plast. 24 (2008) 1071–1096.
[18] V. Tvergaard, A. Needleman, Acta Metall. 32 (1984) 157–169.
[19] A.L. Gurson, J. Eng. Mater. Technol. 99 (1977) 2–15.
[20] J. Besson, R. Foerch, Comput. Method Appl. Mech. Eng. 142 (1997) 165–187.